

Energy-entropy stability of β -plane Kolmogorov flow with drag

Yue-Kin Tsang and William R. Young

Scripps Institution of Oceanography, University of California, San Diego, La Jolla, California 92093, USA

(Received 4 March 2008; accepted 12 June 2008; published online 11 August 2008)

We develop a nonlinear stability method, the energy-entropy (*EZ*) method, that is specialized to two-dimensional hydrodynamics and basic state flows consisting of a single Helmholtz eigenmode. The method is applied to a β -plane flow driven by a sinusoidal body force and retarded by drag with damping time scale μ^{-1} . The standard energy method [H. Fukuta and Y. Murakami, *J. Phys. Soc. Jpn.* **64**, 3725 (1995)] shows that the laminar solution is monotonically and globally stable in a certain portion of the (μ, β) -parameter space. The *EZ* method proves nonlinear stability in a larger portion of the (μ, β) -parameter space than does the energy method. Moreover, by penalizing high wavenumbers, the *EZ* method identifies a most strongly amplifying disturbance that is more physically realistic than that delivered by the energy method. Linear instability calculations are used to determine the region of the (μ, β) -parameter space where the flow is unstable to infinitesimal perturbations. There is only a small gap between the linearly unstable region and the nonlinearly stable region, and full numerical solutions show only small transient amplification in that gap.

© 2008 American Institute of Physics. [DOI: 10.1063/1.2958321]

I. INTRODUCTION

Kolmogorov flow is the simplest example of a two-dimensional motion forced at a single spatial scale. This provides an opportunity to understand the implications of the dual conservation laws of energy and enstrophy, the first of which is Fjørtoft's observation that nonlinear interactions transfer energy simultaneously up and down scale.^{1,2}

The signature of Kolmogorov flow is that motion is maintained against dissipation by a sinusoidal body force. Kolmogorov viewed his problem as an idealized example of a forced-dissipative system in which it might be possible to understand the sequence of bifurcations resulting from increasing the Reynolds number.³ The first steps in this program were an analysis of the viscous linear stability problem.^{4,5} The weakly nonlinear theory, pivoted about the critical Reynolds number $\sqrt{2}$, was subsequently developed.^{6,7}

Laboratory experiments using either soap films,^{8,9} or shallow layers,¹⁰ can be driven by electromagnetic forcing, or by the motion of an enveloping gas, so that the body force approximates a sinusoid. Thus Kolmogorov's problem is also important as an experimentally accessible flow in which aspects of two-dimensional hydrodynamics can be tested. In the laboratory the main dissipative mechanism is drag on the adjacent walls rather than lateral viscosity.^{11,12}

In the geophysical context, the instability of planetary waves on a β -plane^{13–15} is similar to Kolmogorov's problem in many respects. Ekman friction, which is equivalent to sidewall drag in the laboratory, also has a strong effect on the stability of planetary waves.¹⁶

Another geophysical motivation for studying the Kolmogorov problem is the equilibration of baroclinic turbulence. The most unstable mode of baroclinic instability is an exponentially growing sinusoidal flow, which is an exact solution of the equations of motion. The amplitude of this mode is limited by a secondary instability, resembling

Kolmogorov instability. By deflecting energy into the barotropic mode, and hence into zonal jets, this secondary instability equilibrates baroclinic turbulence by direct cascade of the thermal mode to high wavenumbers.¹⁷ Thus weakly nonlinear β -plane Kolmogorov flow has been studied as a model of zonal jet formation in the geophysical context.¹⁸

Our main concern in this investigation is the nonlinear stability analysis of Kolmogorov flow. This avenue was opened by Fukuta and Murakami¹⁹ using the energy method.^{20,21} The energy method provides a sufficient condition for nonlinear stability by finding the critical value of the dissipation ensuring that the disturbance energy decreases *monotonically* to zero. Our interest in this question is whether the second two-dimensional conservation law, namely, squared vorticity or enstrophy, might be used to improve the nonlinear stability results in Ref. 19.

In Sec. II we formulate the Kolmogorov stability problem. In Sec. III we discuss the linear stability of the flow, focusing on the limit in which the drag is much stronger than viscosity. In Sec. IV, we extend the energy-stability condition of Fukuta and Murakami¹⁹ to the β -plane and thus obtain a sufficient condition for nonlinear stability. Comparing the results of Sec. III with those of Sec. IV, we see that there is a region of parameter space in which the flow is linearly stable, but the energy method fails to prove nonlinear stability. In Sec. V we incorporate enstrophy and so develop the energy-entropy (*EZ*) method, which is specialized to two-dimensional hydrodynamics and flows consisting of a single Helmholtz eigenfunction, such as the sinusoidal Kolmogorov flow. The *EZ* method provides a sufficient condition for stability, which is stronger than the energy method, and consequently the gap between the results of linear stability and the nonlinearly stable region of parameter space is narrowed, but not eliminated. Section VI concludes the paper.

II. FORMULATION OF THE STABILITY PROBLEM

With nondimensional variables, the vorticity equation is

$$\nabla^2 \psi_t + J(\psi, \nabla^2 \psi) + \beta \psi_x = \nu \nabla^4 \psi - \mu \nabla^2 \psi + \cos(x - x_f). \quad (1)$$

In Eq. (1) the incompressible velocity field is obtained from a stream function $\psi(x, t)$ according to $(u, v) = (-\psi_y, \psi_x)$. The domain is a doubly periodic square $2\pi L \times 2\pi L$, where L is an integer. The relative vorticity is $\nabla^2 \psi$, where $\nabla^2 \equiv \partial_x^2 + \partial_y^2$ is the two-dimensional Laplacian and $J(a, b) \equiv a_x b_y - a_y b_x$ is the Jacobian. β is the gradient of the Coriolis parameter along y and the two dissipative mechanisms, viscosity ν and drag μ , are represented by the first and second terms on the right hand side of Eq. (1).

The flow in Eq. (1) is forced by a sinusoidal body force, which is the signature of the Kolmogorov flow. In dimensional variables, the Kolmogorov forcing is specified as

$$\tau_f^{-2} \cos[k_f(x - x_f)], \quad (2)$$

where there is a length scale k_f^{-1} and a time scale τ_f . To obtain the nondimensional form in Eq. (1), we have scaled using τ_f and k_f . Thus, if $*$ denotes a dimensional quantity, then in Eq. (1) the nondimensional control parameters are $\beta \equiv \tau_f \beta_* / k_f$, $\mu \equiv \tau_f \mu_*$, $\nu \equiv k_f^2 \tau_f \nu_*$ and $L \equiv k_f L_*$. Also in Eq. (1), the phase $x_f \equiv \tan^{-1}[\beta / (\mu + \nu)]$ is defined so that there is a steady laminar solution

$$\psi_L(x) = -a \cos x, \quad (3)$$

where the amplitude of the laminar flow is

$$a(\beta, \mu, \nu) \equiv \frac{1}{\sqrt{\beta^2 + (\mu + \nu)^2}}. \quad (4)$$

A. Dynamics of the disturbance

The disturbance $\varphi(x, t)$ to the laminar stream function is defined by

$$\psi(x, t) = \psi_L(x) + \varphi(x, t), \quad (5)$$

and the equation of motion of φ is obtained by substituting Eq. (5) into Eq. (1),

$$\begin{aligned} \nabla^2 \varphi_t + J(\varphi, \nabla^2 \varphi) + a \sin x (\nabla^2 \varphi + \varphi)_y + \beta \varphi_x \\ = \nu \nabla^4 \varphi - \mu \nabla^2 \varphi. \end{aligned} \quad (6)$$

The disturbance energy E_φ and enstrophy Z_φ are defined as

$$E_\varphi \equiv \frac{1}{2} \langle |\nabla \varphi|^2 \rangle \quad \text{and} \quad Z_\varphi \equiv \frac{1}{2} \langle (\nabla^2 \varphi)^2 \rangle, \quad (7)$$

where $\langle \cdots \rangle$ denotes spatial average over the whole domain. Multiplying Eq. (6) by φ and averaging gives the disturbance energy equation

$$\frac{dE_\varphi}{dt} = a \langle \varphi_x \varphi_y \cos x \rangle - 2\mu E_\varphi - 2\nu Z_\varphi. \quad (8)$$

Multiplying by $\nabla^2 \varphi$ and averaging produces the disturbance enstrophy equation

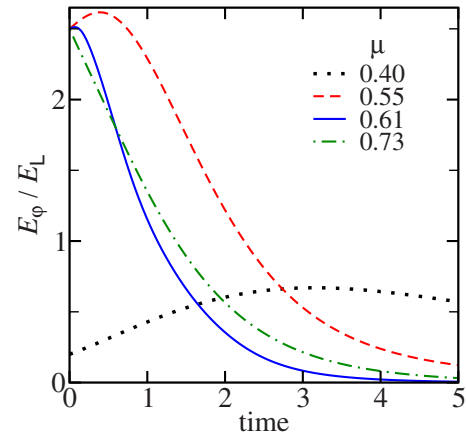


FIG. 1. (Color online) Disturbance energy $E_\varphi(t)$ from the numerical solution of Eq. (1) with $\beta=0$ and $\nu=10^{-3}$. The results are normalized by the laminar energy $E_L = a^2/4$. The solid and dashed curves illustrate the transient growth in E_φ when the laminar solution $\psi_L(x)$ is globally stable, but not monotonically globally stable. The dot-dashed curve illustrates monotonic global stability. The dotted curve shows the development of a linearly unstable perturbation; in this case the ratio $E_\varphi(t)/E_L$ equilibrates at around 0.35 as $t \rightarrow \infty$.

$$\frac{dZ_\varphi}{dt} = a \langle \varphi_x \varphi_y \cos x \rangle - 2\mu Z_\varphi - 2\nu P_\varphi, \quad (9)$$

where $P_\varphi \equiv \frac{1}{2} \langle |\nabla \nabla^2 \varphi|^2 \rangle$ is the disturbance palinstrophy.

It is remarkable that the disturbance energy and disturbance enstrophy are generated at equal rates, i.e., the same source, namely, $a \langle \varphi_x \varphi_y \cos x \rangle$, appears in Eqs. (8) and (9). Thus subtracting Eq. (9) from Eq. (8) gives

$$\frac{1}{2} \frac{d}{dt} (E_\varphi - Z_\varphi) = -\mu (E_\varphi - Z_\varphi) - \nu Z_\varphi + \nu P_\varphi. \quad (10)$$

This cancellation is a general property of flows forced by a single Helmholtz eigenmode and is the basis for recent constraints on the spectral distribution of energy and enstrophy in two-dimensional turbulence.^{22–24} If $\nu=0$ then the solution of Eq. (10) shows that the difference $E_\varphi(t) - Z_\varphi(t)$ decays exponentially to zero. This observation is the basis of the *EZ* method in Sec. V.

B. Linear instability, global stability, and monotonic global stability

Following Joseph,²⁰ we say that the laminar solution $\psi_L(x)$ is *globally stable* if for all initial disturbances

$$\lim_{t \rightarrow \infty} E_\varphi(t) = 0. \quad (11)$$

An even stronger form of stability is *monotonic global stability*, meaning that $dE_\varphi/dt \leq 0$ for all $t \geq 0$. In both cases the laminar solution ultimately attracts all initial conditions.

Global stability does not forbid transient increases in $E_\varphi(t)$, e.g., see Fig. 1. It is a limitation of the standard energy method, reviewed in Sec. IV, that only monotonic global stability can be established. Using the *EZ* method, we show in Sec. V that there is a region of parameter space within

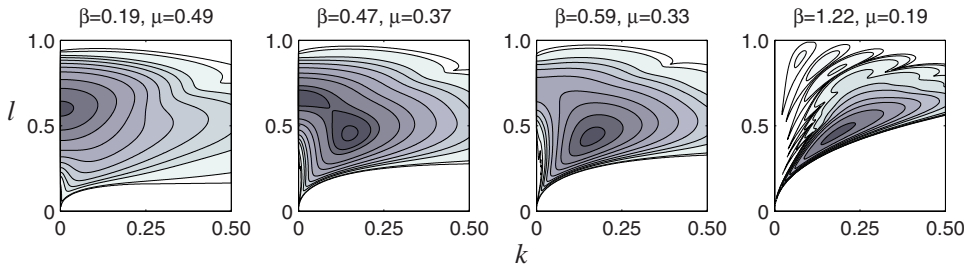


FIG. 2. (Color online) This shows $\max_n \mathcal{J}\{\tilde{\lambda}_n(k, l; \tilde{\beta}, \tilde{\nu}=0)\}$ as a function of k and l ; dark areas are regions of large values. The values of (μ, β) in the titles are obtained by substituting $\tilde{\beta}$ and the peak value, $\tilde{\mu}_{\text{neut}}$, into Eqs. (18a) and (18b).

which Kolmogorov flow is globally stable, but not monotonically globally stable. The solid and dashed curves in Fig. 1 illustrate this situation.

A flow is said to be linearly unstable if the linearized version of Eq. (6) has exponentially growing eigensolutions. This is the subject of Sec. III.

III. LINEAR INSTABILITY

Our goal in this section is to find the “neutral surface” in the (μ, β, ν) -space below which $\psi_L(x)$ is linearly unstable. We linearize Eq. (6) and write φ in the Floquet form:^{12,14}

$$\varphi(x, t) = \Re\{e^{i(kx+ly-\omega t)} \tilde{\varphi}(x)\}, \quad (12)$$

where $-\frac{1}{2} < k \leq \frac{1}{2}$ and $\tilde{\varphi}(x)$ has the same periodicity as $\psi_L(x)$, i.e., $\tilde{\varphi}(x) = \tilde{\varphi}(x+2\pi)$. The resulting eigenproblem is

$$\begin{aligned} [i\tilde{\nu}(D^2 - l^2)^2 + l \sin x(D^2 - l^2 + 1) - i\tilde{\beta}D]\tilde{\varphi} \\ = \tilde{\lambda}(D^2 - l^2)\tilde{\varphi}, \end{aligned} \quad (13)$$

where the differential operator D and the eigenvalue $\tilde{\lambda}$ are

$$D \equiv \frac{d}{dx} + ik, \quad \tilde{\lambda} \equiv \frac{\omega + i\mu}{a}. \quad (14)$$

The two parameters in Eq. (13) are defined as

$$\tilde{\beta} \equiv \frac{\beta}{a}, \quad \tilde{\nu} \equiv \frac{\nu}{a}. \quad (15)$$

The basic flow is linearly unstable if there exists an ω with positive imaginary part, i.e., $\mathcal{J}\{\omega\} = a\mathcal{J}\{\tilde{\lambda}\} - \mu > 0$.

A. Tracing the neutral surface

For a given pair of $(\tilde{\beta}, \tilde{\nu})$, we solve Eq. (13) numerically to obtain the eigenvalue spectrum $\{\tilde{\lambda}_n(k, l; \tilde{\beta}, \tilde{\nu})\}$ as a function of the wavenumber (k, l) . The integer n on $\tilde{\lambda}_n$ indexes the eigenbranch. Once we possess the spectrum, we define the function

$$\tilde{\mu}_{\text{neut}}(\tilde{\beta}, \tilde{\nu}) \equiv \max_{k, l, n} \mathcal{J}\{\tilde{\lambda}_n(k, l; \tilde{\beta}, \tilde{\nu})\}. \quad (16)$$

Figure 2 shows $\max_n \mathcal{J}\{\tilde{\lambda}_n(k, l; \tilde{\beta}, \tilde{\nu})\}$ at four values of μ and β , which happen to fall on the inviscid neutral curve. The function $\tilde{\mu}_{\text{neut}}(\tilde{\beta}, \tilde{\nu})$ in Eq. (16) is obtained by searching through the (k, l) -plane in Fig. 2 to find the maximum.

Because $a\tilde{\mu}_{\text{neut}} - \mu$ is the growth rate of the most unstable mode, the neutral surface in the (μ, β, ν) -space is defined by

$$\mu = a\tilde{\mu}_{\text{neut}}(\tilde{\beta}, \tilde{\nu}). \quad (17)$$

Given $\tilde{\mu}_{\text{neut}}(\tilde{\beta}, \tilde{\nu})$, the neutral surface is traced using the parametric equations

$$\beta = \frac{\tilde{\beta}}{[\tilde{\beta}^2 + (\tilde{\mu}_{\text{neut}} + \tilde{\nu})^2]^{1/4}}, \quad (18a)$$

$$\mu = \frac{\tilde{\mu}_{\text{neut}}}{[\tilde{\beta}^2 + (\tilde{\mu}_{\text{neut}} + \tilde{\nu})^2]^{1/4}}, \quad (18b)$$

$$\nu = \frac{\tilde{\nu}}{[\tilde{\beta}^2 + (\tilde{\mu}_{\text{neut}} + \tilde{\nu})^2]^{1/4}}. \quad (18c)$$

The expressions above follow from Eqs. (4), (15), and (17). The neutral surface is obtained from Eqs. (18a)–(18c) by varying the parameters $(\tilde{\beta}, \tilde{\nu})$ between 0 and ∞ .

B. Gill's inequality

In the inviscid case, $\nu=0$, an argument of Gill¹⁴ and Lorenz¹³ showed that it is sufficient to search for unstable modes within the circle,

$$k^2 + l^2 < 1. \quad (19)$$

In Appendix A we show that Eq. (19) also applies to linearly unstable modes of the viscous problem. Gill's inequality underscores Fj\o rtoft's result¹ by showing that a growing eigenmode must transfer energy to spatial scales that are larger than that of the laminar flow in Eq. (3).

C. The inviscid case, $\nu=0$

The procedure outlined above is particularly simple in the inviscid case $\nu=0$. The inviscid neutral curve in the (μ, β) -plane is the solid curve in Fig. 3. The neutral curve intersects the μ -axis at $\mu=0.52$. After disentangling notational differences, $\mu=0.52$ agrees with Thess's value for unbounded Kolmogorov flow.¹²

An interesting feature of the neutral curve is the appearance of a kink at the point $K: (\mu, \beta) \approx (0.37, 0.46)$. This is due to a change in character of the most unstable mode, evident between the first and third panels of Fig. 2. As one moves along the neutral curve by decreasing μ , the peak eigenvalue on the $k=0$ line is getting smaller and is eventually overtaken by another peak emerging at a location with $k \neq 0$. Consequently the wavenumber k of the most unstable mode discontinuously jumps from $k=0$ to $k=0.15$ at K . Fig-

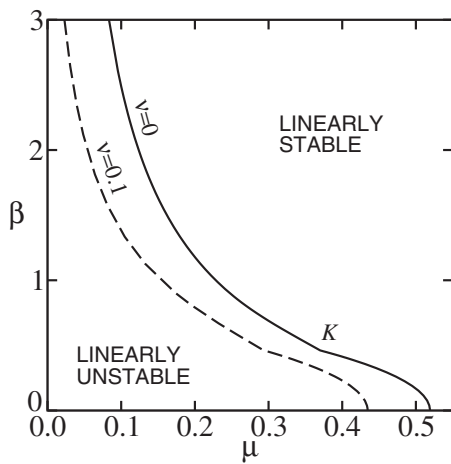


FIG. 3. Results from linear stability analysis of Eq. (1). For the inviscid case $\nu=0$, the solid line is the neutral curve. The point K is where the most unstable mode changes character. For $\nu=0.1$, the dashed line is the neutral curve.

ure 4 shows the transition by plotting the variation of $\tilde{\mu}_{\text{neut}}$ and the wavenumber of the most unstable mode along the neutral curve.

We find that for all growing modes, except for those with $k=0$, the real part of ω is nonzero, $\Re\{\omega\} \neq 0$. Hence the jump in k to a nonzero value as μ decreases also signals that the most unstable mode becomes a traveling wave. In summary, along the neutral curve in Fig. 3, the most unstable modes to the right of point K are stationary disturbances with $k=0$, and those on the left of point K are traveling waves with $k \neq 0$.

We mention that in the inviscid case, the neutral curve can be written as

$$\beta = \sqrt{\frac{\tilde{\mu}_{\text{neut}}^2}{\mu^2} - \mu^2}, \quad (20)$$

and Fig. 4(a) indicates that

$$\tilde{\mu}_{\text{neut}}(\mu) \approx 0.26 - 0.12\mu, \quad 0 < \mu \leq 0.37, \quad (21a)$$

$$\tilde{\mu}_{\text{neut}}(\mu) \approx 0.09 + 0.34\mu, \quad 0.37 < \mu \leq 0.52. \quad (21b)$$

Substituting Eqs. (21a) and (21b) into Eq. (20) gives an approximate expression for the $\nu=0$ neutral curve; this approximation matches the numerical result to within the line width in Fig. 3.

D. The effects of small viscosity

When $\nu \neq 0$, the neutral curve can be traced out by a similar procedure. The dashed curve in Fig. 3 is the result for $\nu=0.1$, showing the stabilizing effect of ν . For $\nu=10^{-3}$, the neutral curve is indistinguishable from the inviscid curve, indicating that the limit $\nu \rightarrow 0$ is nonsingular. We find a kink K in the neutral curve, and a corresponding change in the structure of the most unstable mode always appears at $\beta \sim 0.46$, independent of ν .

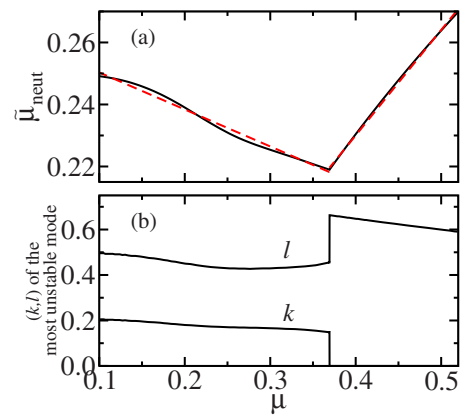


FIG. 4. (Color online) Variation of (a) $\tilde{\mu}_{\text{neut}}$, defined in Eq. (16), and (b) wavenumber (k, l) of the most unstable mode along the linear stability neutral curve. The dashed lines in (a) show the piecewise linear approximation (21a) and (21b).

E. A comment on the viscously controlled limit

In this article we analyze the case of nonzero β and $\mu \gg \nu$, i.e., drag is the main dissipative mechanism. Previously, Manfroi and Young²⁵ discussed the complementary case, $\nu \gg \mu$, in which viscosity controls the instability. These two limits differ qualitatively. The curve with $\nu=0$ in Fig. 3 indicates that the flow is stabilized by increasing β at fixed nonzero μ (even if $\mu \ll 1$). On the other hand, in Ref. 25 it is shown that if ν is below a critical value, then the flow is unstable for any value of β . The viscous limit analyzed in Ref. 25 is singular because the most unstable disturbances spring from the origin of the wavenumber plane. These low-wavenumber disturbances evade the scale-selective damping effect of ν . Fortunately in the case considered here, in which drag is the main dissipative mechanism, everything is simpler: drag acts uniformly on all length scales and thus small-wavenumber disturbances are stabilized. In particular, as shown in Fig. 4(b), the wavenumber of the most unstable disturbances is always nonzero.

IV. THE ENERGY METHOD

We now turn to the stability of the basic flow (3) using the energy method. Fukuta and Murakami¹⁹ have previously considered this problem with $\beta=0$. It is easy to adapt their results to nonzero β because the disturbance energy equation does not involve β : β enters the energy method only through the laminar amplitude, $a(\beta, \mu, \nu)$ in Eq. (4).

We begin by rewriting the disturbance energy equation (8) as

$$\frac{dE_\varphi}{dt} = 2(a\mathcal{R}[\varphi] - \mu)E_\varphi - 2\nu Z_\varphi, \quad (22)$$

where

$$\mathcal{R}[\varphi] \equiv \frac{\langle \varphi_x \varphi_y \cos x \rangle}{\langle |\nabla \varphi|^2 \rangle}. \quad (23)$$

The homogeneous functional \mathcal{R} represents the transfer of energy by Reynolds' stresses between the basic flow and the perturbation flow.

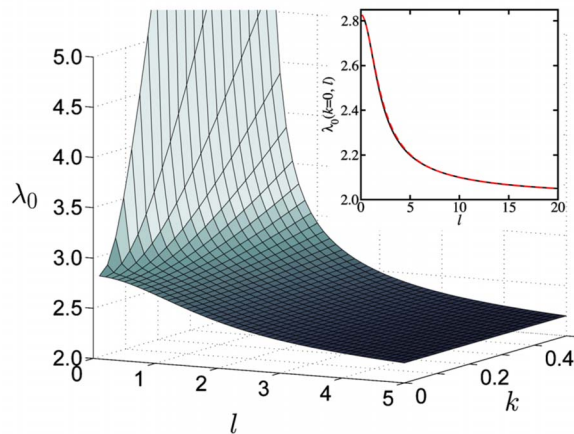


FIG. 5. (Color online) Eigenvalue of the gravest mode of Eq. (29), $\lambda_0(k, l)$. The minimum is at $k=0$ and $l \rightarrow \infty$. The inset shows a cut along $k=0$ (solid line); $\lambda_0(0, l)$ decreases monotonically from $2\sqrt{2}$ at $l=0$ to 2 as $l \rightarrow \infty$. The dashed line is the approximation (B8).

The basic idea of the energy method is that if the dissipative parameters μ and ν are large enough, then the right hand side of Eq. (22) is negative for all possible φ 's (not just φ 's that happen to satisfy the equations of motion). This implies that the disturbance energy decreases monotonically to zero and that the laminar solution is monotonically globally stable.

For instance, since

$$\mathcal{R}[\varphi] \leq \frac{\langle |\varphi_x| |\varphi_y| \rangle}{\langle |\nabla \varphi|^2 \rangle} \leq \frac{1}{2}, \quad (24)$$

it follows from Eq. (22) that

$$\frac{dE_\varphi}{dt} \leq 2 \left(\frac{a}{2} - \mu \right) E_\varphi, \quad (25)$$

and Gronwall's inequality implies that

$$E_\varphi(t) \leq e^{(a-2\mu)t}. \quad (26)$$

That is, if $a < 2\mu$ then the laminar flow in Eq. (3) is monotonically globally stable. This conclusion relies on the seemingly crude inequality in Eq. (24) and one expects that a stronger condition for monotonic global stability might be obtained by working harder and solving the variational problem suggested by maximizing the right hand side of Eq. (22). In this spirit we recapitulate some of the variational results in Ref. 19 by discussing the simplest case $\nu=0$ in some detail.

A. The inviscid case, $\nu=0$

With $\nu=0$, let \mathcal{R}_E be the maximum of $\mathcal{R}[\varphi]$ over all function $\varphi(\mathbf{x})$ satisfying the periodic boundary conditions,

$$\mathcal{R}_E \equiv \max_{\varphi} \mathcal{R}[\varphi]. \quad (27)$$

According to the energy-stability method, the function $\varphi_E(\mathbf{x})$ that maximizes \mathcal{R} is the “most dangerous disturbance,” meaning the most efficient energy-releasing disturbance.

Applying Gronwall's inequality to Eq. (22), if $a\mathcal{R}_E < \mu$ then E_φ decays monotonically to zero and the laminar solu-

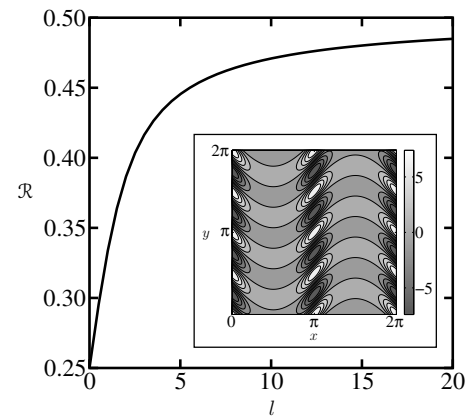


FIG. 6. The functional \mathcal{R} (26) evaluated at the trial function (31) with different l . The inset shows the trial function with $l=4$.

tion is monotonically globally stable. Hence with $\nu=0$, the energy-stability boundary in the (μ, β) -plane is given by $\mu = a\mathcal{R}_E$ or

$$\beta = \sqrt{\frac{\mathcal{R}_E^2}{\mu^2} - \mu^2}. \quad (28)$$

Since $\mathcal{R}[\varphi]$ is a homogeneous functional, we can find \mathcal{R}_E by maximizing $\langle \varphi_x \varphi_y \cos x \rangle$ subject to the constraint $\langle |\nabla \varphi|^2 \rangle = 1$. This leads to the Euler-Lagrange equation

$$(D^2 - l^2)\tilde{\varphi} = i\lambda(\cos x D - \frac{1}{2} \sin x)\tilde{\varphi}, \quad (29)$$

where D is the differential operator defined in Eq. (14) and the Lagrange multiplier appears as a real eigenvalue λ . Then \mathcal{R}_E is given by $1/\lambda_{\min}$, where λ_{\min} is the minimum eigenvalue.

Again we represent φ using the Floquet form in Eq. (12) (but now with $\omega=0$) and solve Eq. (29) numerically to obtain $\lambda_0(k, l)$, the eigenvalue of the gravest mode, as a function of k and l . Figure 5 displays $\lambda_0(k, l)$ above the (k, l) -plane and the conclusion is that

$$\lambda_{\min} = \min_{k, l} \lambda_0(k, l) = 2, \quad (30)$$

with the minimum achieved at $k=0$ and $l \rightarrow \infty$. The numerical result (30) is supported by the analysis of Eq. (29) in Appendix B.

The conclusion $\mathcal{R}_E = 1/\lambda_{\min} = \frac{1}{2}$ is anticipated precisely by the simple inequality in Eq. (24): in the inviscid case the variational solution does not improve the energy-stability boundary at all. The only reward from the variational solution is that it provides the form of the most dangerous disturbance $\varphi_E(\mathbf{x})$. The analysis in Appendix B suggests that this disturbance can be approximated by the trial function

$$\varphi_E(\mathbf{x}) \approx \lim_{l \rightarrow \infty} \cos[l(y + \sin x)] \exp\left(\frac{l}{2} \cos 2x\right). \quad (31)$$

Figure 6 shows that \mathcal{R} evaluated at the trial function above indeed approaches one-half as $l \rightarrow \infty$.

The disturbance shown in the inset of Fig. 6 has the classic form of an optimal perturbation: the disturbance is localized where the base-state shear is a maximum and the

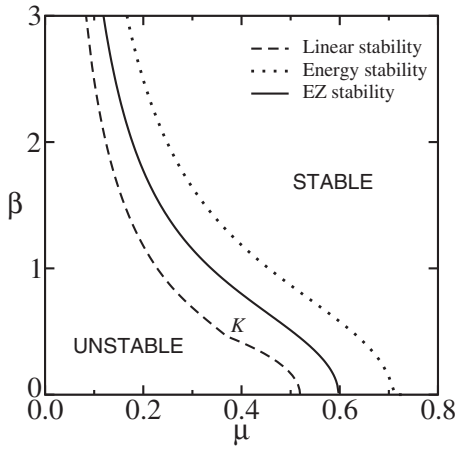


FIG. 7. A summary showing three different stability boundaries for two-dimensional Kolmogorov flow. The dashed curve is the neutral curve of the linear stability documented in Sec. III; the dotted curve is the energy-stability boundary in Eq. (32); the solid curve is the EZ stability boundary in Eq. (40). The point K at $(\mu, \beta) = (0.37, 0.46)$ is where the most unstable linear mode changes from a stationary disturbance to a traveling wave.

disturbance eddies “lean against” the shear.^{26–28} Thus Reynolds’ stresses of the most dangerous disturbance are concentrated in the neighborhood of $\cos x = \pm 1$. Since there is no penalty attached to using very small spatial scales in the functional $\mathcal{R}[\varphi]$, this concentration can be made ever more intense by taking $l \rightarrow \infty$. The trial function shown in the inset of Fig. 6 illustrates this strategy for maximizing $\mathcal{R}[\varphi]$. However, this $\varphi_E(\mathbf{x})$ is realized only in the $l \rightarrow \infty$ limit, and this is distinctly unphysical. This point is discussed further in Sec. V.

With $\mathcal{R}_E = \frac{1}{2}$, it follows from Eq. (28) that the inviscid energy-stability boundary is given by

$$\beta = \sqrt{\frac{1}{4\mu^2} - \mu^2}. \quad (32)$$

Equation (32) is plotted as a dotted curve in Fig. 7. Despite the pathology discussed above, it is remarkable that the energy-stability boundary parallels the linear stability neutral curve of Sec. III even though the parameter β enters the energy method only through the function $a(\beta, \mu, \nu)$ in Eq. (4). This is an indication that the grossest features of the instability are determined by the amplitude of the laminar solution and the disturbance energy equation (22).

B. The viscous case

Turning now to $\nu \neq 0$, the main point of interest is how small viscosity affects the energy-stability curve in Fig. 7. In this case the solution of the variational problem can provide a substantial improvement over the simple inequality (24). Following Fukuta and Murakami,¹⁹ the viscous version of Eq. (29) can be solved numerically and the results are shown in Fig. 8. As $\nu \rightarrow 0$ the energy-stability curves limit to the inviscid curve in Eq. (32). Thus the limit $\nu \rightarrow 0$ is not singular.

One other point of interest is the wavenumber l_* of the most dangerous disturbance. Figure 9 shows the dependence of l_* on ν . In agreement with the small-

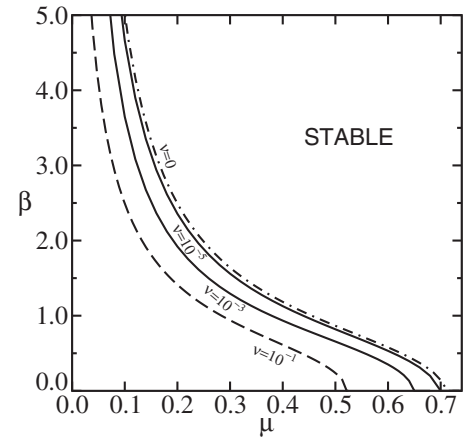


FIG. 8. This shows energy-stability boundaries in the (μ, β) parameter plane. The flow is monotonically globally stable if the parameters (β, μ, ν) locate it above the appropriate curve.

wavenumber expansion,¹⁹ if $\nu/\mu > 0.0204$ then $l_* = 0$ and $\mathcal{R}_E = 1/\sqrt{8(1 + \nu/\mu)}$. Additional asymptotic analysis of ours (not presented here) shows that if $\nu/\mu \ll 0.0204$, then

$$l_* = \left(\frac{\mu}{2\nu}\right)^{1/3} + O(\nu^0). \quad (33)$$

In the limit $\nu \rightarrow 0$ we recover the inviscid result $l_* = \infty$.

V. THE ENERGY-ENSTROPY METHOD

The gap between the neutral curve and the energy-stability boundary in Fig. 7 reflects the stark difference between the linearly unstable eigenmodes and the most efficient energy-releasing disturbance identified by the energy method. Specifically, the wavenumbers of the exponentially growing linear modes satisfy Gill’s inequality (19) while, according to the energy method, the most efficient energy-releasing disturbance has a wavenumber $(k, l) = (0, \infty)$. To improve on the energy method, the energy-enstrophy (EZ) method uses both the disturbance energy and enstrophy.

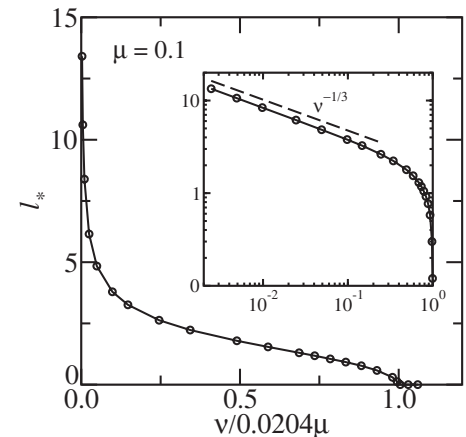


FIG. 9. This shows the dependence of the wavenumber l_* of the most dangerous disturbance on ν . (The most dangerous disturbance has $k_* = 0$ for all ν .) If $\nu \geq 0.0204\mu$ then $l_* = 0$. As ν decreases, l_* increases and ultimately, as shown in the inset, $l_* \sim \nu^{-1/3}$.

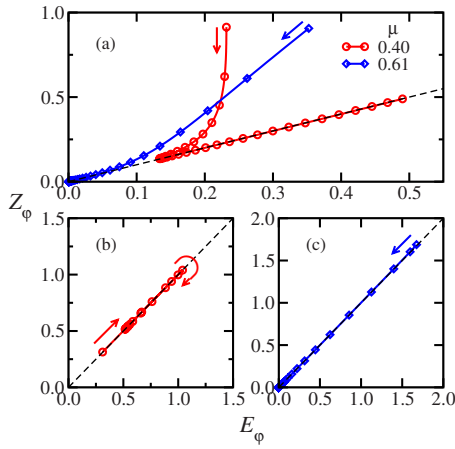


FIG. 10. (Color online) Trajectories of some illustrative solutions of Eq. (6) in the $[E_\varphi(t), Z_\varphi(t)]$ -plane; all solutions have $\beta=0$ and $10^{-3} \leq \nu \leq 5 \times 10^{-3}$. The dashed line marks the set EZ in Eq. (35).

A. The EZ method, $\nu=0$

With $\nu=0$, Eq. (10) implies that

$$E_\varphi(t) - Z_\varphi(t) = e^{-2\mu t} [E_\varphi(0) - Z_\varphi(0)]. \quad (34)$$

Thus, although an arbitrary initial condition may not fall in the set

$$EZ \equiv \{\varphi(x) : E_\varphi = Z_\varphi\}, \quad (35)$$

the solution to Eq. (6) (with $\nu=0$) is attracted by EZ . Moreover, if the initial disturbance does happen to fall within EZ , then it stays within EZ . We refer to initial conditions that fall in EZ as “ EZ -disturbances.”

Figure 10 illustrates the approach to the attracting set EZ using a numerical solution of Eq. (6). Panel (a) shows that solutions starting outside of EZ are quickly attracted to EZ ; panels (b) and (c) show that solutions starting in EZ remain close to EZ . The trajectories with $\mu=0.4$ in panels (a) and (b) show two unstable solutions; nonlinearity halts the growth of the disturbance so that both trajectories asymptote to $(E_\varphi, Z_\varphi) \approx (0.49, 0.49)$ as $t \rightarrow \infty$. The solutions with $\mu=0.61$ in panels (a) and (c) show disturbances whose energy decays monotonically to zero (although $\mu=0.61$ is below the energy-stability boundary). These numerical results, with $0 < \nu \leq \mu$, show that EZ is an attracting set with small but nonzero viscosity.

To obtain an energy-stability bound for EZ -disturbances, we seek

$$\mathcal{R}_{EZ} \equiv \max_{\varphi \in EZ} \mathcal{R}[\varphi]. \quad (36)$$

This is equivalent to maximizing $\mathcal{R}[\varphi]$ in Eq. (23) subject to the constraints

$$\langle |\nabla \varphi|^2 \rangle = \langle (\nabla^2 \varphi)^2 \rangle = 1. \quad (37)$$

The solution $\varphi_{EZ}(x)$ is the most dangerous EZ -disturbance.

The search in Eq. (36) is over a smaller set than the one used to define \mathcal{R}_E in Eq. (27), and so $\mathcal{R}_{EZ} \leq \mathcal{R}_E$. In anticipation of the variational calculation in the next subsection, we remark that

$$\mathcal{R}_{EZ} = 0.3571 < \mathcal{R}_E = \frac{1}{2}. \quad (38)$$

Furthermore, the argument surrounding Eq. (A7) shows that the Floquet wavenumber of an EZ -disturbance must satisfy Gill’s inequality (19). Thus the pathology of the energy method is avoided.

The disturbance energy of an EZ -disturbance satisfies

$$\frac{dE_\varphi}{dt} \leq 2(a\mathcal{R}_{EZ} - \mu)E_\varphi, \quad (39)$$

and Gronwall assured us that the energy decays monotonically to zero provided that $a\mathcal{R}_{EZ} < \mu$. Using the definition of a in Eq. (4), this condition leads to the EZ stability curve

$$\beta = \sqrt{\frac{\mathcal{R}_{EZ}^2}{\mu^2} - \mu^2}, \quad (40)$$

shown as a solid curve in Fig. 7. The trajectories with $\mu=0.61$ in panels (a) and (c) of Fig. 10 show two solutions just to the right of the EZ stability curve in Fig. 7.

In Fig. 7 there is a gap between the EZ curve and the energy-stability curve. In this region EZ -disturbances decay monotonically, while general initial disturbances might have amplifying disturbance energy. In fact, initial amplification can be assured by deploying the trial function on the right of Eq. (31) at $t=0$. We argue heuristically that this amplification can only be transient: Eq. (34) shows that the set in Eq. (35) attracts all initial conditions. Thus, since EZ -disturbances decay monotonically to zero, general initial disturbances will also eventually decay to zero as they evolve toward EZ via Eq. (34). We are arguing heuristically that in the gap between the EZ curve and the energy-stability curve, the laminar solution is globally stable, but not monotonically globally stable.

B. The EZ variational problem

To obtain $\mathcal{R}_{EZ}=0.3571$ in Eq. (38), we maximize $\langle \varphi_x \varphi_y \cos x \rangle$ subject to the constraints that the disturbance enstrophy and energy are both equal to one-half. A direct assault based on solving the Euler–Lagrange equation is described in Appendix C. It is more instructive to develop some intuition using the trial function

$$\varphi = A_0 \cos ly - B_1 \sin ly \sin x, \quad (41)$$

for which

$$\langle \varphi_x \varphi_y \cos x \rangle = \frac{1}{4} l A_0 B_1. \quad (42)$$

With the constraints in Eq. (37), the parameters A_0 and B_1 are expressed in terms of the wavenumber l and substituted into Eq. (42). Thus the trial function in Eq. (41) leads to the estimate

$$\mathcal{R}_{EZ} \approx \max_l l \sqrt{\frac{(1-l^2)}{2(1+l^2)}}. \quad (43)$$

The maximum of the right hand side is $1-2^{-1/2}=0.293\dots$, which is achieved at $l^2 = \sqrt{2}-1$. This is a lower bound on \mathcal{R}_{EZ} .

TABLE I. The estimate of \mathcal{R}_{EZ} in the final column quickly converges to the numerical value indicated in Eq. (38) as more terms in the Fourier series (44) are retained.

A_0	A_2	A_4	B_1	B_3	l	\mathcal{R}_{EZ}
1.4142	1.2872	...	0.6436	0.2929
2.1561	0.2764	...	1.3010	...	0.4253	0.3556
2.2141	0.2694	...	1.2983	0.0371	0.4171	0.3571
2.2175	0.2689	0.0037	1.2984	0.0376	0.4166	0.3571

To more closely approximate \mathcal{R}_{EZ} we generalize Eq. (41) to

$$\varphi = \cos ly \sum_{n=0}^{\infty} A_{2n} \cos 2nx - \sin ly \sum_{n=0}^{\infty} B_{2n+1} \sin(2n+1)x. \quad (44)$$

Table I summarizes the result of retaining more terms in the Fourier series (44). Optimization over A_n , B_n , and l provides an estimate of \mathcal{R}_{EZ} that quickly converges to the numerical value indicated in Eq. (38). Figure 11 illustrates the most dangerous EZ -disturbance calculated using the final row of Table I.

C. Limitations of the EZ method

The EZ method as presented above applies only to basic states consisting of a single Helmholtz eigenmode, i.e., only if the laminar solution satisfies

$$\nabla^2 \psi_L + k_f^2 \psi_L = 0. \quad (45)$$

The sinusoidal Kolmogorov flow in Eq. (3) is the simplest and most widely studied member of this class.

To appreciate the necessity of Eq. (45), consider the evolution of nonlinear disturbances to a general basic state $\psi_L(x, y)$. The evolution equation for the disturbance is

$$\begin{aligned} \nabla^2 \varphi_t + J(\psi_L, \nabla^2 \varphi) + J(\varphi, \zeta_L) + J(\varphi, \nabla^2 \varphi) + \beta \varphi_x \\ = \nu \nabla^4 \varphi - \mu \nabla^2 \varphi, \end{aligned} \quad (46)$$

where $\zeta_L \equiv \nabla^2 \psi_L$ is the vorticity of the laminar solution. For a general flow the disturbance energy and enstrophy, defined in Eq. (7), satisfy

$$\frac{dE_\varphi}{dt} = -\langle \psi_L J(\varphi, \nabla^2 \varphi) \rangle - 2\mu E_\varphi - 2\nu Z_\varphi \quad (47)$$

and

$$\frac{dZ_\varphi}{dt} = \langle \zeta_L J(\varphi, \nabla^2 \varphi) \rangle - 2\mu Z_\varphi - 2\nu P_\varphi. \quad (48)$$

The EZ method relies on forming a linear combination of Eqs. (47) and (48) that eliminates the $J(\varphi, \nabla^2 \varphi)$ -source terms on the right. This is straightforward if ψ_L satisfies Eq. (45): then the source terms cancel exactly and $Z_\varphi - k_f^2 E_\varphi$ decays exponentially as in Eq. (34) (provided that $\nu=0$). Thus only in this ‘‘Helmholtz case’’ one can proceed by maximizing the relevant Reynolds’ functional—the analog of $\mathcal{R}[\varphi]$ in Eq. (23)—within the set EZ .

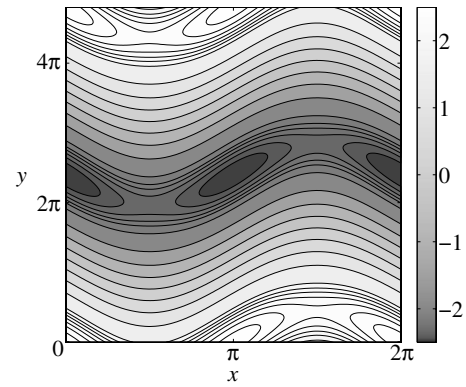


FIG. 11. The most dangerous EZ -disturbance (47) calculated using the final row of Table I.

VI. CONCLUSION AND DISCUSSION

We have studied the instability of geophysical ($\beta \neq 0$) Kolmogorov flow and focused on the limit in which drag is much stronger than viscosity, $\mu \gg \nu$. We show that the form of the fastest exponentially growing eigenmodes changes abruptly from stationary disturbances to traveling waves as one moves along the neutral curve in the (μ, β) -plane. In this sense, β strongly affects the instability. Nonetheless, the stability boundary obtained by the energy method¹⁹ is reasonably close, and parallel, to the linear stability neutral curve. Because β enters the energy method only through the amplitude of the laminar solution, i.e., $a(\beta, \mu, \nu)$ in Eq. (4), this success indicates that the main features of the instability are determined by the amplitude of the laminar solution, a , and the disturbance energy equation.

It is striking that the most unstable inviscid disturbance identified by the energy method is unphysical because it is strictly realized only in the infinite wavenumber limit, $l \rightarrow \infty$. Despite this issue, the energy method still delivers a useful sufficient condition for global monotonic stability.

In Sec. V, we extend the energy method by incorporating information based on the disturbance enstrophy equation. For Helmholtz flows satisfying Eq. (45), the EZ method results in a third stability boundary that lies closer to the neutral curve than does the energy-stability boundary. One might therefore conclude that the additional information provided by enstrophy produces only a quantitative narrowing of the gap between energy stability and linear stability. However the main interest in the EZ method is the identification of EZ -disturbances in Eq. (35) and then calculation of the most unstable disturbance within EZ . Unfortunately for general laminar flows it does not seem to be possible to identify a set analogous to EZ .

The various types of stability we have discussed here characterize the neighborhood of the laminar solution $\psi_L(x)$ in Eq. (3). However Doering and Constantin^{29,30} have recently devised a variational procedure in which notions of energy stability are applied to statistically steady turbulent flow. This results in bounds on important large-scale quantities, such as the mechanical energy dissipation and the heat flux. A motivation for this paper has been the possibility of applying or generalizing the technique of Doering and

Constantin to two-dimensional turbulence. In this context it is essential to take account of enstrophy conservation, perhaps via the notion of *EZ* stability.

ACKNOWLEDGMENTS

This work was supported by the National Science Foundation by Grant Nos. OCE07-26320 and OCE02-20362.

APPENDIX A: EXTENSION OF GILL'S INEQUALITY TO INCLUDE VISCOSITY

Gill's inequality in Eq. (19) restricts the Floquet wavenumber of an exponentially growing eigenmode to lie within the unit circle in the (k, l) -plane. To prove this result, observe that a growing eigenmode of the Floquet form (12) satisfies Eq. (10). Thus

$$(\omega_i + \mu)[E_\varphi(0) - Z_\varphi(0)] = \nu P_\varphi(0) - \nu Z_\varphi(0), \quad (\text{A1})$$

where $\omega_i \geq 0$ is the imaginary part of ω and $E_\varphi(0)$, etc., is the initial energy, etc., of the eigenmode.

The disturbance enstrophy can be written as

$$Z_\varphi = -\frac{1}{2} \langle \nabla \varphi \cdot \nabla \nabla^2 \varphi \rangle, \quad (\text{A2})$$

so that the Cauchy–Schwarz inequality implies

$$Z_\varphi^2 \leq P_\varphi E_\varphi. \quad (\text{A3})$$

Replacing $P_\varphi(0)$ in Eq. (A1) by $Z_\varphi^2(0)/E_\varphi(0)$, we obtain an inequality equivalent to

$$\left(\omega_i + \mu + \nu \frac{Z_\varphi(0)}{E_\varphi(0)} \right) [E_\varphi(0) - Z_\varphi(0)] \geq 0. \quad (\text{A4})$$

The first factor is non-negative, and consequently a growing eigenmode must have more energy than enstrophy,

$$E_\varphi(0) \geq Z_\varphi(0). \quad (\text{A5})$$

In the inviscid case considered by Gill¹⁴ the result (A5) is an equality following immediately from Eq. (A1) without the Cauchy–Schwarz excursion.

To obtain the inequality (19), substitute the Floquet form (12), with

$$\tilde{\varphi}(x) = \sum_{n=-\infty}^{\infty} \varphi_n e^{inx}, \quad (\text{A6})$$

into Eq. (A5),

$$\sum_{n=-\infty}^{\infty} (1 - h_n^2) h_n^2 |\varphi_n|^2 \geq 0. \quad (\text{A7})$$

Above $h_n^2 \equiv (k+n)^2 + l^2$ is the wavenumber of the n th wave in the Floquet series. Recalling that $-1/2 < k \leq 1/2$, it is easy to see that $1 - h_n^2$ is negative if $|n| \geq 2$. Consequently the inequality above can only be satisfied because $1 - h_0^2$ or $1 - h_{\pm 1}^2$ are positive. This requirement implies Eq. (19).

APPENDIX B: THE INVISCID ENERGY-STABILITY EIGENPROBLEM

In this appendix we use perturbation theory to analyze the eigenproblem (29) in various limits. The analysis can be simplified by the transformation¹⁹

$$\tilde{\varphi}(x) = \exp\left[\frac{i l \lambda \sin x}{2}\right] \theta(x). \quad (\text{B1})$$

This results in

$$\frac{d^2 \theta}{dx^2} + 2ik \frac{d\theta}{dx} + \left[l^2 \left(\frac{\lambda^2}{4} \cos^2 x - 1 \right) - k^2 \right] \theta = 0. \quad (\text{B2})$$

Fukuta and Murakami¹⁹ solved Eq. (B2) for the gravest eigenmode in the small wavenumber limit,

$$\theta = 1 + \frac{1}{4}(k^2 + l^2) \cos 2x - \frac{1}{8}ik(k^2 + l^2) \sin 2x + O(k, l)^4, \quad (\text{B3})$$

with the corresponding gravest eigenvalue

$$\frac{\lambda_0^2}{4} \approx \left(1 + \frac{k^2}{l^2} \right) \left(2 - \frac{k^2 + l^2}{4} \right) + O(k, l)^4. \quad (\text{B4})$$

This shows that as $(k, l) \rightarrow (0, 0)$, with $l \neq 0$, $\lambda_0 \rightarrow 2\sqrt{2}$.

We now consider the complementary case $k=0$ and $l \gg 1$; we define a small parameter by $\epsilon^2 \equiv l^{-1}$. Numerical solution of Eq. (B2) indicates that the minimum of $\lambda_0(k, l)$ is at $\lambda_0(0, \infty) = 2$ and we are seeking some analytic assurance of this hypothesis. The eigenfunction is concentrated in the neighborhood of $x=0$, where $\lambda^2/4 \cos^2 x - 1$ in Eq. (B2) is slightly positive. Thus we expand $\cos^2 x \approx 1 - x^2 + O(x^4)$ and introduce a boundary-layer coordinate $X = x/\epsilon$ so that Eq. (B2) reduces to

$$\theta_{XX} + \left(\frac{\lambda^2 - 4}{4\epsilon^2} - \frac{\lambda^2}{4} X^2 \right) \theta = O(\epsilon^2). \quad (\text{B5})$$

We recognize the quantum harmonic oscillator equation and thus obtain the eigenvalues as

$$\frac{\lambda_n^2 - 4}{2\lambda_n \epsilon^2} = 2n + 1, \quad n = 0, 1, 2, \dots \quad (\text{B6})$$

Hence, the eigenvalue of the gravest mode ($n=0$) is

$$\lambda_0 \approx 2 + l^{-1} + O(l^{-2}), \quad (\text{B7})$$

and $\lambda_0 \rightarrow 2$ as $l \rightarrow \infty$.

The expression

$$\frac{\lambda_0^2}{4} = 1 + \frac{\sqrt{1 + c^2 l^2}}{1 + c l^2}, \quad c = 1 - 2^{-1/2} = 0.2928 \dots, \quad (\text{B8})$$

agrees with Eq. (B4) when $k=0$ and $l \ll 1$, and with Eq. (B7) if $k=0$ and $l \gg 1$. The inset of Fig. 5 shows that the interpolation (B8) is a good approximation to the numerically computed eigenvalues for all l .

The algebraic form of the trial function in Eq. (31) is suggested by the perturbation theory in this appendix. The factor $\cos[l(y + \sin x)]$ corresponds to $\exp(i l y)$ times the factor $\exp(i l \lambda \sin x / 2)$ in Eq. (B1) (using $\lambda=2$ as the optimal

choice). The other factor in Eq. (31), namely, $\exp(\frac{1}{2}l \cos 2x)$, is an interpolant to $\theta(x)$ which has the correct structure as $l \rightarrow 0$ and as $l \rightarrow \infty$.

APPENDIX C: THE EZ EULER-LAGRANGE EQUATION

The direct approach to solve the EZ variational problem in Sec. V B is to include the two constraints (37) using two Lagrange multipliers p and q . Thus setting the variational derivative of

$$\langle \varphi_x \varphi_y \cos x \rangle - q \langle |\nabla \varphi|^2 \rangle + p [\langle |\nabla \varphi|^2 - (\nabla^2 \varphi)^2 \rangle] \quad (\text{C1})$$

to zero results in the Euler-Lagrange equation

$$p \nabla^4 \varphi + (p - q) \nabla^2 \varphi = \frac{1}{2} \varphi_y \sin x - \varphi_{xy} \cos x. \quad (\text{C2})$$

Multiplying Eq. (C2) by φ and taking the spatial average, we deduce that

$$q = \langle \varphi_x \varphi_y \cos x \rangle. \quad (\text{C3})$$

Writing φ in the Floquet form (12) (with $\omega=0$), we solve Eq. (C2) by regarding p as an eigenvalue and q as a parameter for different values of k and l satisfying Gill's inequality (19). For a given q , admissible solutions are the subset of eigenfunctions of Eq. (C2) that satisfies

$$\frac{\langle |\nabla \varphi|^2 \rangle}{\langle (\nabla^2 \varphi)^2 \rangle} - 1 = 0. \quad (\text{C4})$$

\mathcal{R}_{EZ} , defined in Eq. (38), is then given by the maximum q at which such solutions exist. Now, we know that

$$0.3571 \leq q \leq 0.5. \quad (\text{C5})$$

The upper limit is what we get if we ditch the enstrophy constraint and perform the maximization within the larger class of functions satisfying only $\langle |\nabla \varphi|^2 \rangle = 1$. The lower limit is obtained from the trial function method described in Sec. V B. Thus, we only need to search for \mathcal{R}_{EZ} within the range in Eq. (C5). The result is $\mathcal{R}_{EZ} = 0.3571$ with $p = 0.0069$ and $(k, l) = (0, 0.4166)$. These numbers are virtually the same as the trial function result given in the final row of Table I. We observe that in both the energy method and the EZ method, the most unstable disturbance has wavenumber $k=0$. Unfortunately we have not been able to prove this result analytically.

¹R. Fjørtoft, "The changes in the spectral distribution of kinetic energy for two dimensional nondivergent flow," *Tellus* **5**, 225 (1953).

²P. E. Merilees and H. Warn, "On energy and enstrophy exchanges in two-dimensional non-divergent flow," *J. Fluid Mech.* **69**, 625 (1975).

³V. I. Arnol'd, "Kolmogorov's hydrodynamic attractors," *Proc. R. Soc. London, Ser. A* **434**, 19 (1991).

⁴L. D. Meshalkin and Y. G. Sinai, "Investigation of the stability of a stationary solution of a system of equations for the plane movement of an incompressible viscous liquid," *J. Appl. Math. Mech.* **25**, 1700 (1961).

⁵J. S. A. Green, "Two-dimensional turbulence near the viscous limit," *J. Fluid Mech.* **62**, 273 (1974).

⁶A. A. Nepomnyashchy, "On the stability of the secondary flow of a viscous liquid in an infinite domain," *J. Appl. Math. Mech.* **40**, 836 (1976).

⁷G. I. Sivashinsky, "Weak turbulence in periodic flows," *Physica D* **17**, 243 (1985).

⁸M. Rivera and X. L. Wu, "External dissipation in driven two-dimensional turbulence," *Phys. Rev. Lett.* **85**, 976 (2000).

⁹J. M. Burgess, C. Bizon, W. D. McCormick, J. B. Swift, and H. L. Swinney, "Instability of the Kolmogorov flow in a soap film," *Phys. Rev. E* **60**, 715 (1999).

¹⁰N. F. Bondarenko, M. Z. Gak, and F. V. Dolzhansky, "Laboratory and theoretical models of a plane periodic flow," *Izv. Akad. Nauk SSSR, Fiz. Atmos. Okeana* **15**, 1017 (1979).

¹¹F. V. Dolzhansky, "On the influence of external friction on stability of plane parallel flows of homogeneous incompressible fluid," *Izv. Akad. Nauk SSSR, Fiz. Atmos. Okeana* **23**, 348 (1987).

¹²A. Thess, "Instabilities in two-dimensional spatially periodic flows. Part I: Kolmogorov flow," *Phys. Fluids A* **4**, 1385 (1992).

¹³E. N. Lorenz, "Barotropic instability of Rossby wave motion," *J. Atmos. Sci.* **29**, 228 (1972).

¹⁴A. E. Gill, "The stability of planetary waves on an infinite beta-plane," *Geophys. Fluid Dyn.* **6**, 29 (1974).

¹⁵Y. Lee and L. M. Smith, "Stability of Rossby waves in the beta-plane approximation," *Physica D* **179**, 53 (2003).

¹⁶F. V. Dolzhansky, "Effect of Ekman layer on the stability of planetary waves," *Izv. Akad. Nauk SSSR, Fiz. Atmos. Okeana* **21**, 292 (1985).

¹⁷R. Salmon, "Baroclinic instability and geostrophic turbulence," *Geophys. Astrophys. Fluid Dyn.* **15**, 167 (1980).

¹⁸A. J. Manfroi and W. R. Young, "Slow evolution of zonal jets on the beta plane," *J. Atmos. Sci.* **56**, 784 (1999).

¹⁹H. Fukuta and Y. Murakami, "Nonlinear stability of Kolmogorov flow with bottom-friction using the energy method," *J. Phys. Soc. Jpn.* **64**, 3725 (1995).

²⁰D. D. Joseph, *Stability of Fluid Motions I*, 1st ed. (Springer-Verlag, Berlin, 1976).

²¹P. G. Drazin and W. H. Reid, *Hydrodynamic Stability*, 2nd ed. (Cambridge University Press, Cambridge, 2004).

²²P. Constantin, C. Foias, and O. P. Manley, "Effects of the forcing function spectrum on the energy spectrum in 2-D turbulence," *Phys. Fluids* **6**, 427 (1994).

²³C. V. Tran and T. G. Shepherd, "Constraints on the spectral distribution of energy and enstrophy dissipation in forced two-dimensional turbulence," *Physica D* **165**, 199 (2002).

²⁴A. Alexakis and C. R. Doering, "Energy and enstrophy dissipation in steady state 2d turbulence," *Phys. Lett. A* **359**, 652 (2006).

²⁵A. J. Manfroi and W. R. Young, "Stability of beta-plane Kolmogorov flow," *Physica D* **162**, 208 (2002).

²⁶W. Orr, "Stability or instability of the steady motions of a perfect fluid," *Proc. R. Ir. Acad., Sect. A* **27**, 9 (1907).

²⁷B. Farrell, "Developing disturbances in shear," *J. Atmos. Sci.* **44**, 2191 (1987).

²⁸R. Iacono, "Local energy generation in barotropic flows," *J. Atmos. Sci.* **59**, 2153 (2002).

²⁹C. R. Doering and P. Constantin, "Energy dissipation in shear driven turbulence," *Phys. Rev. Lett.* **69**, 1648 (1992).

³⁰C. R. Doering and P. Constantin, "Variational bounds on energy dissipation in incompressible flows: Shear flow," *Phys. Rev. E* **49**, 4087 (1994).